Confinement properties of a $Ga_{0.25}In_{0.75}As/InP$ quantum point contact

T. P. Martin,[1,2,*] C. A. Marlow,[2] L. Samuelson,[3] A. R. Hamilton,[1] H. Linke,[2] and R. P. Taylor[2,4]
[1]*School of Physics, University of New South Wales, Sydney NSW 2052, Australia*
[2]*Department of Physics, University of Oregon, Eugene, Oregon 97403, USA*
[3]*Division of Solid State Physics, Lund University, P.O. Box 118, S-221 00 Lund, Sweden*
[4]*Department of Physics and Astronomy, University of Canterbury, Christchurch 8140, New Zealand*
(Received 25 September 2007; revised manuscript received 31 January 2008; published 8 April 2008)

We study the electrostatic confinement properties of a ballistic GaInAs nanostructure, a system with a high potential for quantum applications due to its small effective mass and persistence of quantum effects to higher temperatures. By measuring the magnetic depopulation of one-dimensional subbands in an etched quantum point contact, we demonstrate that the slope of the confinement at the Fermi level is an order of magnitude steeper than in surface-gated devices, indicating that this system is ideal for applications that are sensitive to the boundary geometry of devices. The subband spacing is found to range from 7 to 9.5 meV, which is significantly larger than previously reported for this material system.

DOI: 10.1103/PhysRevB.77.155309 PACS number(s): 73.21.Hb, 73.40.Qv, 75.47.Jn

I. INTRODUCTION

Quantum confinement of a two-dimensional electron gas (2DEG) has been used for remarkably diverse investigations, ranging from fundamental physics (e.g., fractionally charged quasiparticles[1] and quantum chaos[2]) to potential device applications (e.g., electron coherence[3] and spintronics[4]). The devices responsible for this success are traditionally defined by patterned surface gates in $Al_xGa_{1-x}As/GaAs$ heterostructures. However, $Ga_xIn_{1-x}As$ heterostructures have been increasingly utilized for electron transport studies in low-dimensional systems recently, especially in the areas of quantum coherence and spintronics. The reduced effective mass of GaInAs ($\sim$0.04–0.05 compared to 0.067 for GaAs) leads to enhanced confinement and the potential for higher operational temperatures due to the larger associated energy level spacings. Large spin-orbit coupling parameters measured for GaInAs have also made it a viable candidate for the control of spin procession.[5,6] Crucially, in this paper, we demonstrate that the electrostatic confinement potentials produced by etching nanostructures into this heterostructure are an order of magnitude steeper than for gated devices—opening up the possibility of higher fidelity patterning, which is critical for many classical and phase-coherent device applications. A number of such applications have already utilized etched devices in GaInAs; examples include phase coherence studies in quantum dots,[7,8] fractal analysis of quantum interference,[9] and symmetry studies in quantum billiards.[10,11] In all of these studies, inherent assumptions are made regarding the confinement in these devices, as the confinement properties of GaInAs nanostructures have not been previously explored in detail.

In this paper, we investigate the confinement potential in etched GaInAs devices by utilizing the magnetic depopulation of one-dimensional (1D) subbands in a quantum point contact (QPC). Etched QPCs have been demonstrated to have 1D subband spacings on the order of 10 meV,[12,13] more than double those found in surface-gated QPCs.[14,15] Here, we establish that these large subband spacings are also achievable in a GaInAs heterostructure. Using a uniform top gate to tune the Fermi energy relative to the subbands of the QPC, we perform magnetic depopulation measurements to determine the 1D subband spacing ΔE_n and the shape of the confining potential.[16,17] We model the depopulation in the QPC using a "bathtub" potential[16,17] and match the output of this model to the measured physical depopulation. This enables us to extract parameters that determine the physical confinement while keeping the measurement in the linear response regime.

II. EXPERIMENT

Our QPC is etched into a strained $Ga_{0.25}In_{0.75}As/InP$ heterostructure,[18,19] as shown schematically in the inset of Fig. 1. The heterostructure is grown using metal-organic vapor phase epitaxy onto a substrate of semi-insulating (100) InP:Fe.[18] It consists of a 9 nm wide $Ga_{0.25}In_{0.75}As$ quantum well ($m^*=0.047m_0$) (Ref. 18) situated between a 50 nm buffer layer and a 41 nm capping layer of nonintentionally doped InP. The midpoint of the capping layer is delta doped ($\sim$1 nm) with Si donors at a density of 5×10^{18} cm^{-3}. The

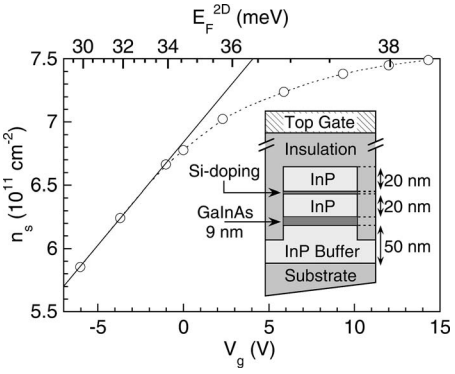

FIG. 1. Carrier density n_s in the 2D reservoirs plotted as a function of gate voltage V_g (lower axis) and the Fermi energy E_F^{2D} in the 2DEG (upper axis). The solid line shows the linear trend at negative voltages; at positive voltages, n_s departs from this trend and saturates. Inset: schematic of the heterostructure.

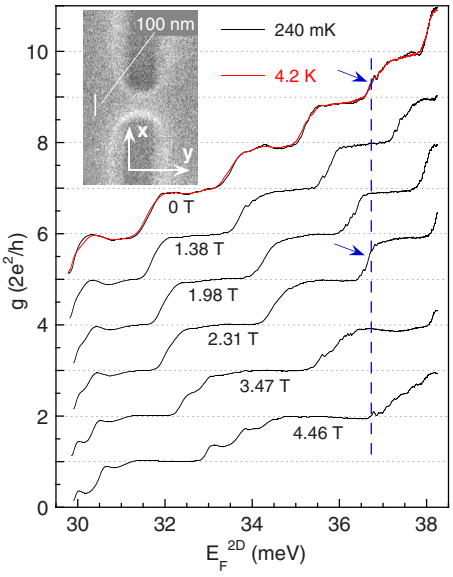

FIG. 2. (Color online) Conductance g through the QPC plotted vs the Fermi energy E_F^{2D} in the 2DEG for selected magnetic fields B. As B increases, the subband transitions move to higher energy. The data are offset for clarity by multiples of $2e^2/h$. Black traces are measured at 240 mK, the red trace at 4.2 K. Inset: scanning electron microscopy image of the QPC.

QPC is located on a Hall bar mesa featuring NiAuGe Ohmic contacts and is defined using electron-beam lithography and a nonselective HBr wet etch (see Fig. 2, inset). A 1 μm thick layer of hard-baked Shipley 1813 photoresist is used to fill the etch trenches, passivate the heterostructure, and electrically insulate the heterostructure from the Ti/Au top gate. This insulating layer limits the gate leakage current to <10 pA. Further details of the fabrication can be found elsewhere.[18,19] All measurements were performed in a four-terminal configuration using standard ac-lock-in techniques at 37 Hz, with a constant current of $\lesssim 1$ nA to prevent electron heating.

Figure 1 shows the carrier density n_s in the 2DEG as a function of gate voltage V_g, obtained from measurements of the Shubnikov–deHaas (SdH) oscillations and the low-field Hall slope. Within the voltage range of Fig. 1, the mobility and mean free path vary between $(1.5-2.5)\times 10^5$ cm^2/V s and $2-4$ μm, respectively, indicating ballistic transport through our ~ 160 nm long QPC. For an ideal metal-insulator-semiconductor device structure, the top gate and 2DEG interact as a simple capacitor producing a linear relationship between n_s and V_g. In our device, while linear behavior is observed at negative V_g, n_s saturates at positive V_g. The region of saturation at $V_g>0$ suggests that charge is building up somewhere between the 2DEG and the gate, limiting the gate's ability to modify n_s. Likely causes for this saturation include interface traps[20] between the capping layer and the photoresist, or a repopulation of the Si donor sites. Measurements of the longitudinal resistivity reveal that the SdH oscillations fall to zero and there is no noticeable positive magnetoresistance,[21] suggesting the absence of parallel conduction in the measurement.[22] Based on these observations, we assume that the charge causing the saturation does not contribute to conduction measurements in our device and that the only mobile charge is in the quantum well. A detailed analysis of the cause of the saturation is reported elsewhere.[21]

The saturation at $V_g>0$ signifies a nonlinear relationship between V_g and the Fermi energy, as shown in the upper axis of Fig. 1. In Fig. 2, the conductance g through the QPC is plotted as a function of the Fermi level E_F^{2D} in the 2DEG reservoirs. By plotting the data vs E_F^{2D} instead of vs V_g, we are able to bypass this spurious saturation and chart g relative to the movement of the Fermi level. The conductance measured at $B=0$ and $T=240$ mK is shown in the upper trace (black) of Fig. 2. Plateaus at integer values of $2e^2/h$ appear as E_F^{2D} is increased and rises through the 1D subbands of the QPC.[23] The same measurement at $T=4.2$ K is shown superimposed (red) over the trace at 240 mK. The transitions between plateaus at 4.2 K show little deviation from those at 240 mK, suggesting that the subband spacing in our QPC is larger than a few meV.[23] Note that while the data in Fig. 2 and our subsequent analysis are presented for a particular QPC, it is consistent with measurements we have made in other etched QPCs in this heterostructure.[9]

We use magnetic depopulation of the subbands in the QPC to determine ΔE_n and to characterize the electrostatic confinement potential. Applying a magnetic field B perpendicular to the 2DEG strengthens the confinement in the QPC, moving the subband transitions to higher energy (see Fig. 2). As B is increased, lower indexed subbands eventually coincide with higher indexed subbands at the same value of E_F^{2D}. This is emphasized by the blue dashed line in Fig. 2, and it is schematically represented in Fig. 3(a), where the $n=5$ subband at 0 T and the $n=4$ subband at 2.31 T align at an identical value of E_F^{2D}. Under the assumption that the bottom of the conduction band is insensitive to changes in B, the *minima* of the potentials at $B=0$ and 2.31 T must also align in energy. Thus, a calculation of the two subband energies that coincide at E_F^{2D} in Fig. 3(a) must result in identical values E_F^{1D} (where E_F^{1D} is the Fermi energy in the QPC). This calculation can be used to constrain a model of the electrostatic confinement.[16,17] To more easily identify the values of B at which subbands coincide, in Fig. 3(b), we replot the depopulation points from Fig. 2 on a parameter space of E_F^{2D} and B. We neglect the effects of spin splitting and assume the subband crossings occur half-way between the spin-resolved transitions in Fig. 2; the error bars in Fig. 3(b) represent the strength of the Zeeman splitting for these transitions.

III. RESULTS AND DISCUSSION

To extract the form of the confinement potential from the magnetic depopulation data in Fig. 3(b), we assume a model potential and constrain this model by calculating the subband energies that coincide in E_F^{2D}. It is well established that the form of the confining potential in a 1D constriction evolves from a parabolic potential at depletion to a flat bottomed parabola when populated by electrons.[24] Therefore, we choose a bathtub as our model potential [see Fig. 3(a)], which is characterized by a flat, central valley of width d situated between regions of harmonic confinement of frequency ω_0,[16,17]

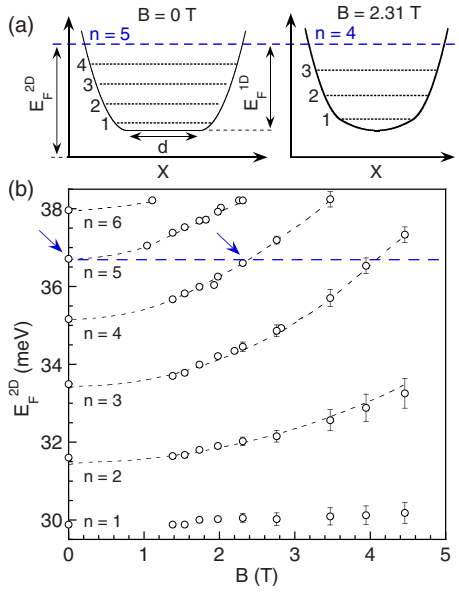

FIG. 3. (Color online) (a) Schematic of the confinement potential plotted vs distance x across the QPC for $B=0$ and 2.31 T. The additional confinement due to B raises the subbands to higher energy. (b) Parameter-space plot of the subband transitions: Fermi energy E_F^{2D} in the 2DEG vs magnetic field B. Black dashed lines are fits to the data based on the bathtub model. Blue arrows point to the values of B at which the $n=5$ and $n=4$ subbands are coincident in E_F^{2D}, as schematically depicted in (a).

$$V(E_F^{2D},x) = \begin{cases} 0, & |x| \le \frac{d}{2} \\ \frac{1}{2}m^*\omega_0^2\left(|x| - \frac{d}{2}\right)^2, & |x| > \frac{d}{2}. \end{cases} \quad (1)$$

Note that ω_0 and d will, in general, depend on E_F^{2D}. The subband energies are calculated by inserting $V(E_F^{2D},x)$ into the Schrödinger equation, which is numerically solved using the finite difference method with ω_0 and d as fitting parameters. For a given value of E_F^{2D}, *three* coincident subband transitions are necessary to uniquely determine these parameters. This condition is satisfied for $n \geqslant 5$ in Fig. 3(b), and we calculate $\hbar\omega_0 = 11.5 \pm 1$ meV for this region of the parameter space. For $n < 5$ where there are at most two coincident subbands, we assume ω_0 to be fixed[17] and use d as the fit parameter. This is consistent with the calculations of Laux *et al.*,[24] where the harmonic part of the confinement (i.e., the walls) was found to be insensitive to changes in the subband population and carrier density n_{1D} in the constriction.

In Figs. 4(a)–4(c), we plot the Fermi level E_F^{1D} in the QPC, the width d, and n_{1D} as a function of E_F^{2D} for $\hbar\omega_0 = 10.5$, 11.5, and 12.5 meV. The carrier density n_{1D} is calculated from the 1D density of states and E_F^{1D} at $B=0$ T. Figures 4(a) and 4(c) reveal that E_F^{1D} and n_{1D} are insensitive to changes in ω_0 within the range of our uncertainty. Note that E_F^{1D} will not necessarily be the same as E_F^{2D} [see Fig. 3(a)], since the conduction band bends up within the QPC to form a barrier. The energy of this barrier, $E_{bar} = E_F^{2D} - E_F^{1D}$, directly follows from the solutions to our model. Symbols in Fig. 4

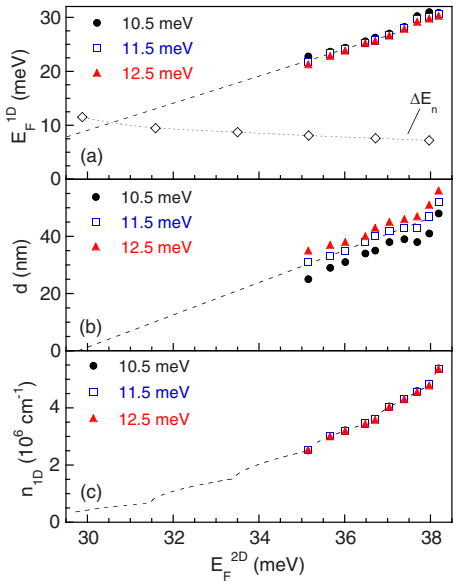

FIG. 4. (Color online) (a) Fermi energy E_F^{1D}, (b) width d of the bathtub's flat region, and (c) carrier density n_{1D} in the QPC plotted vs the Fermi energy E_F^{2D} in the 2DEG. Symbols correspond to different $\hbar\omega_0$. The dashed lines in (a) and (b) are extrapolated trends based on the data, while the dashed line in (c) is calculated from the trends in (a) and (b). Open diamonds in (a) plot the subband spacing ΔE_n.

correspond to the values of E_F^{2D} where at least two subband crossings are coincident. Taking the median value $\hbar\omega_0 = 11.5$ meV, we linearly extrapolate the trends in Figs. 4(a) and 4(b) down to the $n=1$ transition. The trend in Fig. 4(b) extrapolates to $d=0$ at about the same value of E_F^{2D} at which the $n=1$ transition occurs. This is consistent with the bathtub model, where the flat region should disappear once n_{1D} is entirely depleted from the QPC. Finally, we use the data and extrapolated trends in Figs. 4(a) and 4(b) to simulate the subband transitions in the parameter space of Fig. 3(b), plotted there as dashed lines. Despite being derived from a linear extrapolation, the simulated trends for the $n=2$ and $n=3$ subbands reproduce the data with a fair amount of accuracy. However, our model breaks down at the $n=1$ transition because E_F^{1D} extrapolates to a value above what is expected for $\hbar\omega_0 = 11.5$ meV.

The agreement between our model and the experimental data in Fig. 3(b) suggests that our model potential is a good approximation to the confinement in the QPC for $n > 1$. Thus, we use this model to estimate a number of important transport parameters in the QPC as a function of E_F^{2D}: the subband spacing, the electrostatic width, and the slope of the confinement at the Fermi level. The subband spacing at the Fermi level ΔE_n is plotted in Fig. 4(a) and ranges from 7 to 9.5 meV as the subbands are depopulated from $n=6$ to $n=2$. These values are consistent with the temperature dependence observed for the subband transitions at $B=0$ T in Fig. 2. They are also significantly larger than the subband spacing of 2.5 meV previously measured using a biasing technique for a quantum wire of similar width (~100 nm) etched into the same heterostructure.[25] This discrepancy is

explained by noting that in Ref. 25 the quantum wire was overgrown with InP, which is expected to eliminate interface states at the etch boundary and result in a square-well confinement. In our QPC, interface states are expected to deplete the constriction causing an increase in confinement. This depletion strengthens as the subbands are depopulated, resulting in an electrostatic width that can range from 50 to 100 nm at the Fermi level. Note that a bias measurement of our subband spacing would require large biases (~10 meV) relative to the Fermi energy (~30 meV), which can place the measurement outside of linear response.[26] A detailed analysis of biasing in this regime will be presented elsewhere.

We find that the slope of our confinement potential ranges from 1.5 to 2.2 meV/nm at the Fermi level, which is an order of magnitude steeper than found for surface-gated confinement in GaAs.[27] This suggests that nanostructures etched into our heterostructure will have better shape fidelity, where the shape of the electrostatic confinement more accurately conforms to a lithographic pattern. For example, the corners of a square or triangle will be less rounded. This is consistent with the results from recent studies of nonlinear and asymmetric transport in ballistic quantum billiards,[10,11] where the transport dynamics were shown to be very sensitive to the boundary shape. Enhanced control over the boundary shape is particularly important to transport through open quantum dots,[32] where it is well known that curvature in the device geometry produces chaotic orbits[28,29] that limit the dwell time of carriers in the dot.[8,30] Sharper boundary features can introduce stable orbits into a dot's classical phase space, which can lead to dynamical tunneling[31] and an enhancement of the dwell time. We emphasize that the steeper confinement should result from the etched nature of the device, as opposed to being specific to GaInAs, and thus steeper profiles can be expected in other etched heterostructures such as AlGaAs/GaAs. We also stress that we observe an order of magnitude enhancement despite the presence of depletion at the boundaries of the constriction—which we attribute to charge states at the etched boundary.

IV. CONCLUSION

In summary, we have determined the confinement properties of an etched quantum point contact in a $Ga_{0.25}In_{0.75}As/InP$ heterostructure by utilizing the depopulation of the device conductance as a function of the Fermi level and a perpendicular magnetic field. By modeling the confinement as a bathtub potential, we obtain close agreement between the measured points of depopulation and those predicted by our model. The subband spacing in our QPC is calculated to range from 7 to 9.5 meV, which is similar to that observed for etched QPCs in AlGaAs/GaAs heterostructures.[12,13] The slope of the confinement at the Fermi level is found to be an order of magnitude steeper than in surface-gated devices, indicating that etched GaInAs heterostructures will be beneficial for applications requiring smaller and better defined nanostructures.

ACKNOWLEDGMENTS

We thank A. P. Micolich and T. M. Fromhold for useful discussions. We acknowledge financial support by the National Science Foundation (T.P.M., C.A.M., and H.L.), the Research Corporation (R.P.T.), and the Australian Research Council (A.R.H.).

*tmartin@phys.unsw.edu.au

[1] Y. Ji, Y. Chung, D. Sprinzak, M. Heiblum, D. Mahalu, and H. Shtrikman, Nature (London) **422**, 415 (2003).
[2] A. P. Micolich, R. P. Taylor, A. G. Davies, J. P. Bird, R. Newbury, T. M. Fromhold, A. Ehlert, H. Linke, L. D. Macks, W. R. Tribe *et al.*, Phys. Rev. Lett. **87**, 036802 (2001).
[3] J. J. Lin and J. P. Bird, J. Phys.: Condens. Matter **14**, R501 (2002).
[4] J. A. Folk, R. M. Potok, C. M. Marcus, and V. Umansky, Science **299**, 679 (2003).
[5] T. Schäpers, J. Knobbe, and V. A. Guzenko, Phys. Rev. B **69**, 235323 (2004).
[6] S. A. Studenikin, P. T. Coleridge, and P. J. Poole, Semicond. Sci. Technol. **28**, 1103 (2005).
[7] B. Hackens, F. Delfosse, S. Faniel, C. Gustin, H. Boutry, X. Wallart, S. Bollaert, A. Cappy, and V. Bayot, Phys. Rev. B **66**, 241305(R) (2002).
[8] B. Hackens, S. Faniel, C. Gustin, X. Wallart, S. Bollaert, A. Cappy, and V. Bayot, Phys. Rev. Lett. **94**, 146802 (2005).
[9] C. A. Marlow, R. P. Taylor, T. P. Martin, B. C. Scannell, H. Linke, M. S. Fairbanks, G. D. R. Hall, I. Shorubalko, L. Samuelson, T. M. Fromhold *et al.*, Phys. Rev. B **73**, 195318 (2006).
[10] A. Löfgren, I. Shorubalko, P. Omling, and A. M. Song, Phys. Rev. B **67**, 195309 (2003).
[11] C. A. Marlow, R. P. Taylor, M. Fairbanks, I. Shorubalko, and H. Linke, Phys. Rev. Lett. **96**, 116801 (2006).
[12] A. Kristensen, J. B. Jensen, M. Zaffalon, C. B. Sorensen, S. M. Reimann, M. Michel, and A. Forchel, J. Appl. Phys. **83**, 607 (1998).
[13] S. F. Fischer, G. Apetrii, U. Kunze, D. Schuh, and G. Abstreiter, Nat. Phys. **2**, 91 (2006).
[14] R. Taboryski, A. Kristensen, C. B. Sørensen, and P. E. Lindelof, Phys. Rev. B **51**, 2282 (1995).
[15] K. J. Thomas, M. Y. Simmons, J. T. Nicholls, D. R. Mace, M. Pepper, and D. A. Ritchie, Appl. Phys. Lett. **67**, 109 (1995).
[16] K.-F. Berggren, T. J. Thornton, D. J. Newson, and M. Pepper, Phys. Rev. Lett. **57**, 1769 (1986).
[17] D. A. Wharam, U. Ekenberg, M. Pepper, D. G. Hasko, H. Ahmed, J. E. F. Frost, D. A. Ritchie, D. C. Peacock, and G. A. C. Jones, Phys. Rev. B **39**, 6283 (1989).
[18] P. Ramvall, N. Carlsson, P. Omling, L. Samuelson, W. Seifert, Q. Wang, K. Ishibashi, and Y. Aoyagi, J. Appl. Phys. **84**, 2112 (1998).
[19] P. Ramvall, N. Carlsson, I. Maximov, P. Omling, L. Samuelson, W. Seifert, Q. Wang, and S. Lourdudoss, Appl. Phys. Lett. **71**, 918 (1997).

[20] P. Viktorovitch, J. Electrochem. Soc. **136**, 1431 (1989).
[21] T. P. Martin, C. A. Marlow, L. Samuelson, H. Linke, and R. P. Taylor, Physica E (Amsterdam) **40**, 1754 (2008).
[22] M. J. Kane, N. Apsley, D. A. Anderson, L. L. Taylor, and T. Kerr, J. Phys. C **18**, 5629 (1985).
[23] C. W. J. Beenakker and H. van Houten, Solid State Phys. **44**, 1 (1991).
[24] S. E. Laux, D. J. Frank, and F. Stern, Surf. Sci. **196**, 101 (1988).
[25] Q. Wang, N. Carlsson, I. Maximov, P. Omling, L. Samuelson, W. Seifert, W. Sheng, I. Shorubalko, and H. Q. Xu, Appl. Phys. Lett. **76**, 2274 (2000).
[26] L. Martín-Moreno, J. T. Nicholls, N. K. Patel, and M. Pepper, J. Phys.: Condens. Matter **4**, 1323 (1992).
[27] A. P. Micolich, R. P. Taylor, A. G. Davies, T. M. Fromhold, H. Linke, L. D. Macks, R. Newbury, A. Ehlert, W. R. Tribe, E. H. Linfield *et al.*, Appl. Phys. Lett. **80**, 4381 (2002).
[28] R. A. Jalabert, H. U. Baranger, and A. D. Stone, Phys. Rev. Lett. **65**, 2442 (1990).
[29] C. M. Marcus, A. J. Rimberg, R. M. Westervelt, P. F. Hopkins, and A. C. Gossard, Phys. Rev. Lett. **69**, 506 (1992).
[30] Y. Alhassid, Rev. Mod. Phys. **72**, 895 (2000).
[31] A. P. S. de Moura, Y.-C. Lai, R. Akis, J. P. Bird, and D. K. Ferry, Phys. Rev. Lett. **88**, 236804 (2002).
[32] By "open," we refer to dots with coupling leads that have fully conducting modes.